

Provided for non-commercial research and education use.
Not for reproduction, distribution or commercial use.



This article appeared in a journal published by Elsevier. The attached copy is furnished to the author for internal non-commercial research and education use, including for instruction at the authors institution and sharing with colleagues.

Other uses, including reproduction and distribution, or selling or licensing copies, or posting to personal, institutional or third party websites are prohibited.

In most cases authors are permitted to post their version of the article (e.g. in Word or Tex form) to their personal website or institutional repository. Authors requiring further information regarding Elsevier's archiving and manuscript policies are encouraged to visit:

<http://www.elsevier.com/copyright>



ELSEVIER

doi:10.1016/j.ultrasmedbio.2008.12.013

● *Original Contribution*

PROPAGATION OF VIBRATION CAUSED BY ELECTRICAL EXCITATION IN THE NORMAL HUMAN HEART

HIROSHI KANAI

Graduate Schools of Engineering and Biomedical Engineering, Tohoku University, Sendai, Japan

(Received 12 August 2008, revised 3 December 2008, in final form 16 December 2008)

Abstract—The ability to noninvasively detect regional dynamic myocardial damage related to action potentials and mechanical properties affected by heart disease is of great clinical importance. Though there are invaluable clinical tools for diagnosis of a broad range of cardiac conditions, such myocardial properties cannot be evaluated. We have previously shown that pulsive vibration occurs on the myocardium after electrical stimulation of an isolated heart. In this study, using a novel technique for ultrasonic measurement of the myocardial motion, we detected pulsive vibrations spontaneously caused by electrical excitation and by valve closure. Using a sparse sector scan, the vibrations were measured almost simultaneously at about 10,000 points set in the heart wall at a high temporal resolution. The consecutive spatial distributions of the phase of the vibrations revealed wave propagation along the wall in healthy subjects for the first time *in vivo*. At around the time of the Q-wave of the electrocardiogram, the propagation started from the interventricular septum and extended to both the base and apical sides of the heart with a speed of 1 m/s, which corresponds to the propagation of electrical excitation from the Purkinje fiber-myocyte junction in the interventricular septum. Other vibrations then propagated from the base at several m/s, although some of them had dispersion properties. These are shear waves caused by the mitral-valve closure, corresponding to the first heart sound. These phenomena have potential for detection of regional myocardial tissue damage related to propagation of the action potentials and regional myocardial viscoelasticity. (E-mail: hkanai@ecei.tohoku.ac.jp) © 2009 World Federation for Ultrasound in Medicine & Biology.

Key Words: Echocardiography, Action potentials, Elasticity, Imaging, Shear waves, Electrocardiogram.

INTRODUCTION

Though electrocardiography (ECG) has become an invaluable clinical tool for diagnosis of a broad range of cardiac conditions, the regional properties of the myocardium can still not be directly measured noninvasively. Many research reports on the physiologic properties of the heart conduction system have been published but almost all of them have concerned animals or isolated human hearts (Durrer et al. 1970). If the propagation of electrical excitation and mechanical vibration in the heart wall could be directly visualized, regional tissue damage related to both ion channel gating, which generates the electrical action potentials and the regional myocardial mechanical properties due to heart diseases could be thoracically detected. Recently, imaging of epicardial potentials by a combination of electrocardiographic imaging and heart-torso geometry obtained by computed

tomography (CT) has become possible by placement of many electrodes on the surface of the human body (Ramanathan et al. 2004). Though the electrophysiologic activation sequence during activation and repolarization can be noninvasively reconstructed, the mapping is restricted to the surface of the heart.

We have previously found that pulsive vibration occurs in response to electrical stimulation of the extracted myocardium of a rat (Kanai et al. 2003). The amplitude was minute, *i.e.*, about 30 μm in displacement and 0.5 mm/s in vibration velocity. Though the delay times in both the generated force and the change in thickness in response to the electrical stimulation were long at about 100 ms, the delay in the vibration velocity was short at about 15–30 ms. Therefore, transcutaneous measurement of the minute vibration caused by the electrical excitation has potential to reveal the propagation of the electrical excitation in the heart wall *in vivo*.

Typical imaging tools, namely, magnetic resonant imaging (MRI), X-ray computed tomography (CT) and conventional echocardiography, enable clinical visualization of cross-sectional images of the human heart. Moreover, the left ventricular (LV) volume, motion and

Address correspondence to: Hiroshi Kanai, Ph.D., Graduate Schools of Engineering and Biomedical Engineering, Tohoku University, 6-6-05 Aramaki-aza-Aoba, Sendai 980-8579, Japan. E-mail: hkanai@ecei.tohoku.ac.jp

torsional deformation during contraction have been noninvasively measured by CT (Mahoney et al. 1987), two-dimensional (2D) echocardiography (Notomi et al. 2005) and tissue tagging MRI (Axel et al. 1989; Buchalter et al. 1990). However, the temporal resolution in MRI is inevitably limited by the relaxation time (about 14–25 ms) of the tissue in response to the magnetic excitation (Zwanenburg et al. 2004). The time resolution is 13 ms (Wyman et al. 1999a). The in-plane spatial resolution is 1.25×3 mm and the slice thickness is 7 mm (Wyman et al. 1999b). As a characteristic timing parameter of cardiac contraction, the time to onset of circumferential shortening was measured with MRI tagging (Wyman et al. 1999a), in which the time to onset of activation was determined by the time when the strain due to contraction has a maximum, at least several tenths of a microsecond after the pacing. The tissue Doppler imaging (TDI) technique (Sutherland et al. 1994; Fleming et al. 1994; Heimdal et al. 1998)—modified 2D color flow mapping—has been developed to accurately measure myocardial velocity. This technique is still restricted to static configurations or large motion (>1 mm) with low frequency components (<30 Hz) because the detectable amplitude is greater than the wavelength (about $400 \mu\text{m}$ at 3.75 MHz) and the temporal resolution is at most 16 ms. Therefore, it has been considered that there are no minute vibrations with high frequency components in the actual human heart walls and none of these conventional clinical imaging methodologies can detect minute vibrations of the myocardium caused by electrical excitation and valve closure nor visualize myocardial dynamic properties with high temporal resolution of a few milliseconds.

To measure the original wall vibrations of the heart sounds, which are audible by a stethoscope, we have developed a novel ultrasound-based transthoracic method to measure the minute vibrations in the heart wall as waveforms and to show their spatial distribution (Kanai et al. 1996, 1999a, 1999b). The measurement of the vibration is simultaneously applied to several thousand points preset at $51.3\text{-}\mu\text{m}$ intervals along about 10 ultrasonic beams, which are scanned sparsely in the heart wall to maintain a high frame rate (Kanai et al. 2001). The spatial distribution with regard to the waveform or the instantaneous phase of the specific frequency component is shown at every 2 ms, precisely revealing the propagation of the vibration waves on the ultrasonic cross-sectional plane of the heart wall (Kanai 2005).

By applying this novel method to healthy human subjects, we have previously found that some impulsive vibrations, which correspond to the second heart sound, are mechanically caused by closure of the heart valves (Kanai et al. 2000) and propagate along the heart wall with frequency dispersion (Kanai 2005). Their characteris-

tics were found to agree with the theoretical characteristics of the Lamb wave, a kind of the shear plate wave. In healthy human subjects, we have detected vibrations corresponding to the response of the myocardium to electrical excitation (Kanai 2007). However, dispersion properties and transmural propagation were not shown. Similar results have been obtained in an animal study (Pernot et al. 2007; Konofagou 2007) in which acquisition at a depth of about 10 mm was applied to small animals to realize an equivalently high frame rate (8 kHz) with the ECG gating, that is, its measurement continued during several heartbeats, by referring to the R-waves, the measured waveform was divided into several heartbeats and, then, the cross-sectional image of the instantaneous displacements was reconstructed in one cardiac cycle. In a recent article (Wang et al. 2008), this method was applied to the left ventricle of a human subject. However, based on the ECG-gating technique, showing the results was restricted to the period after the R-wave. Thus, the wave propagation from the time of the Q-wave to the time of the R-wave was not shown and the wave propagation could not be analyzed for each frequency component.

In the present study, this novel method was applied to healthy human hearts to reveal the propagation and dispersion properties of the myocardial vibrations caused by electrical excitation both in the base-apex and transmural directions. Furthermore, regarding the mechanical vibrations caused by valve closure, which correspond to the first heart sound, the present study revealed that there are several components which propagate at different speeds.

To understand the following discussion, it may be helpful to recall that the P-wave of the electrocardiogram is the electrical trigger for mechanical contraction of the atria, while the QRS-complex is the electrical trigger for mechanical contraction of the ventricles. The first heart sound follows the QRS-complex and is traditionally thought to be primarily associated with vibrations resulting from the closure of the tricuspid and mitral valves. The second heart sound usually follows the T-wave and is thought to be primarily associated with vibrations resulting from the closure of the pulmonary and aortic valves. The techniques and results presented below permit one to visualize subtle features of specific mechanical vibrations occurring during the propagation of the electrochemical depolarization wave responsible for the surface electrocardiogram. Timing points such as T_Q , corresponding to the Q-wave of the surface electrocardiogram, and T_I and T_{II} , the time of first and second heart sounds, respectively, are employed in the following discussion.

MATERIALS AND METHODS

According to a novel ultrasonic-based method—the phased tracking method (Kanai et al. 1996, 1999a)—the rapid vibration in the heart wall is measured as

a waveform as follows. RF pulses are transmitted from an ultrasonic transducer at a pulse repetition interval ΔT and the reflected ultrasonic wave is received by the same transducer and is multiplied by the original RF signal for quadrature-demodulation. A complex cross-correlation technique is employed to determine the phase shift $\Delta\theta(t)$ between the consecutively obtained resultant signals. Since $\Delta\theta(t)$ corresponds to the displacement $\Delta x(t)$ during the short-period ΔT , the average velocity during the period is estimated by $v(t) = \Delta x(t)/\Delta T$. By accumulating the instantaneous displacement estimate $\Delta x(t)$, the large motion $x(t)$ due to the heartbeat is tracked over one heartbeat (Kanai et al. 1997; Yoshiara et al. 2007) and the minute vibration component $v(t)$ superimposed on $x(t)$ is simultaneously obtained as a waveform. Since the high frequency components contained in the velocity waveform $v(t)$ are suppressed by the integration, the equivalent time resolution of the resultant displacement wave $x(t)$ decreases. Therefore, the velocity waveform $v(t)$ is of concern in the present study. When the maximum measurable depth d_{\max} is 100 mm from the chest surface and the sound speed c_0 is 1540 m/s, the repetition pulse interval ΔT should be equal to or shorter than $2d_{\max}/c_0 \cong 130 \mu\text{s}$. The upper limit $|v_{\max}|$ of the vibration measurement is given by

$$|v_{\max}| = c_0 \frac{\pi}{4\pi f_0 \Delta T} \approx 0.79 \text{ m/s}, \quad (1)$$

where the frequency f_0 of the ultrasound is assumed to be 3.75 MHz. A minute phase change $\Delta\theta(t)$ of 0.4 degrees caused by displacement during ΔT can be accurately determined by introducing a constraint, namely, that their waveforms are identical but their phase values change (Kanai et al. 1996, 1999a). The achieved lower limit $|v_{\min}|$ in the velocity measurement has been validated as being about 0.1 mm/s, which was confirmed in phantom experiments (Kanai et al. 1997) and which corresponds to $0.13 \mu\text{m}$ in displacement. The wavelength is about $410 \mu\text{m}$ for the typical frequency (3.75 MHz) applied to the human heart. Thus, the measurable displacement on the order of $0.13 \mu\text{m}$ corresponds to about 1/3000 of the wavelength. It is difficult to achieve such minute displacement with the conventional speckle tracking method when the maximum amplitude of the cross-correlation function of the RF signals is detected. On the other hand, for the conventional Doppler method, the large motion is not tracked and thus the displacement and the velocity of the same point cannot be measured. Thus, such a minute vibration superimposed on the large motion cannot be noninvasively measured by any other method.

To simultaneously measure the vibrations at many points in the interventricular septum (IVS), ultrasonic

diagnostic equipment (SSD6500; Aloka Co. Ltd., Tokyo, Japan) was modified so that N scan lines with different directions from a sector scanner could be arbitrarily selected in real time (Kanai 2005; Kanai et al. 2000). The number, N , of directions should be increased as much as possible so as to increase the spatial resolution. However, the actual maximum velocity $|v_{\text{act}}|$ of the vibration at the points in the IVS of the human heart is about 0.07 m/s (Kanai et al. 1996, 1999a) in a typical case, which is about 1/10.7 of $|v_{\max}|$. That is, the maximum number N_{\max} of the beam directions is given by dividing $|v_{\max}|$ of eqn 1 by $|v_{\text{act}}|$,

$$N_{\max} = \frac{|v_{\max}|}{|v_{\text{act}}|} \approx 10. \quad (2)$$

Thus, about 10 appropriate directions ($N = 10$) are sparsely selected from the 240 directions addressable in the phased-array ultrasonic probe as illustrated by the narrow fan-shaped area at the center of Fig. 1a. Along each scan line, the RF signal is acquired at a sampling frequency f_s of 15 MHz and, thus, many points at intervals of $c_0/f_s = 51.3 \mu\text{m}$ are set from the apical side to the base side in the IVS. The spatial resolution along the ultrasonic beam depends mainly on the length of the transmitted ultrasonic pulse, which is a few times the wavelength (about $410 \mu\text{m}$) of the employed frequency of 3.75 MHz. By applying the above procedure to each j -th point preset along the k -th scan line, the vibrations at several thousand points, $\{v_{j,k}(t)\}$ ($j = 1, 2, \dots; k = 1, 2, \dots, N$), are simultaneously measured.

If the propagation speed of the detected pulsive wave is 7 m/s for a 50 Hz component, its wavelength is 14 cm, which is comparable to the size of the whole heart and, thus, its propagation phenomenon along the heart wall cannot be easily visualized by showing the amplitude of the pulsive wave. Instead, the phase value of the pulsive wave, which varies from 0 to 360 degrees within one wavelength, is effective for such visualization. The phase value $\varphi_{j,k}(t; f_1)$ of the measured wave $v_{j,k}(t)$ for a frequency f_1 is obtained by applying a short-time Fourier transform with a Gaussian window. From the results obtained at multiple frequencies $\{f_1\}$, the dispersion property of the propagation of the detected vibration is shown. For a frequency less than 20 Hz, however, the length of the Gaussian window would have to be long, precluding detection of change in the propagation phenomena. For the frequency components higher than 60 Hz, the signal-to-noise ratio was rather poor. Thus, the frequencies $\{f_1\}$ at 40 Hz and 40 ± 16 Hz were selected. In the actual experiments, instead, 21 Hz, 41 Hz and 55 Hz were replaced by the respective values closest to the discrete frequencies determined by the window length. The total

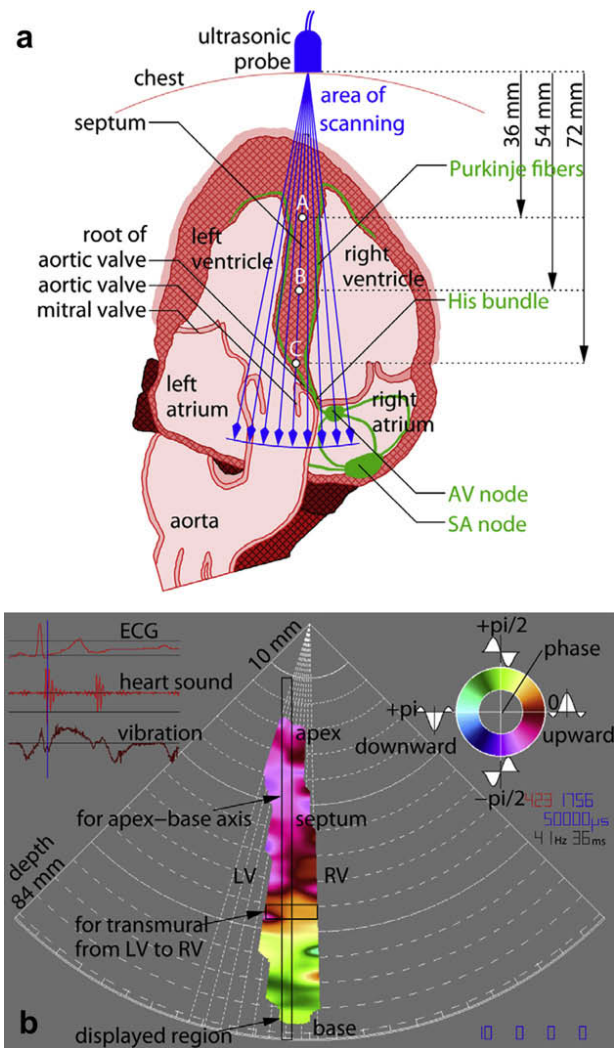


Fig 1. (a) Illustration showing a typical cross-sectional image of the heart in the apical view acquired by a conventional ultrasound diagnostic system. The fan-shaped region corresponds to the sparse scanning range of the ultrasonic beams in the present measurements. The conduction system from the sinoatrial (SA) node through the atrio-ventricular (AV) node and His bundle to the Purkinje network, shown by green lines, transmits the cardiac impulse almost simultaneously to the entire right and left ventricular endocardia. (b) Example of the spatial distributions of color-coded phase values of the 42 Hz component in the waveforms of Fig. 2. The region surrounded by the upright thin black rectangle for each time was cut out and set in an array to show consecutive spatial distributions of color-coded phase values of the waveforms along the center of the IVS around T_R , as shown in the upper panel of each of Figs. 4, 6 and 7. The region surrounded by the horizontal black rectangle was cut out, rotated by -90 degrees, and set in an array to show the transmural distributions from the LV side to the RV side around T_R as shown in the lower panel of each of Fig. 4a through c.

length of the Gaussian window was ± 72 ms, but its amplitude parameter was set so that the amplitude at ± 36 ms decreased to 3.5% of that at the window center.

Since the amplitude at ± 8.2 ms decreased to 50% of that at the window center using this setting, the equivalent time resolution of Fourier analysis was about 16 ms. The underlying hypothesis for the frequency analysis is that the spectrum does not change during the equivalent period.

The phase value $\varphi_{j,k}(t; f_1)$ is color-coded based on the upper-right circular illustration in Fig. 1b for imaging of 2D spatial distribution $\{\varphi_{j,k}(t; f_1)\}$ ($j = 1, 2, \dots$) (Kanai 2005; Kanai et al. 2000). An example of this is shown in Fig. 1b. The detected phase value $\varphi_{j,k}(t; f_1)$ corresponds to the delay time of the specific frequency component from the center of the short time window. By shifting the time t of the window by about 2 ms, the same analysis is consecutively applied. By this procedure, minute vibrations $\{v_{j,k}(t)\}$ are simultaneously detected at many points in the heart wall and the spatial distribution of their phase components, $\{\varphi_{j,k}(t; f_1)\}$, are consecutively obtained with high time resolution, which is sufficient to visualize the propagation of the wave caused by electrical excitation and that of mechanical vibration in the heart wall. In the present study, this method was applied to three normal young male volunteers. The study was approved by the review committee of the Graduate School of Engineering, Tohoku University and the healthy subjects gave informed consent.

RESULTS

Figure 2 shows a typical example of the vibration waveforms, $v_A(t)$, $v_B(t)$ and $v_C(t)$, for a subject at three points—(A) apical side, (B) middle and (C) base side—set on an ultrasonic beam passing through the IVS between the left ventricle (LV) and the right ventricle (RV), as illustrated in Fig. 1. Though four consecutive heartbeats were overlaid, there was high reproducibility in succeeding cardiac cycles. Around the radiation time (T_I) of the first heart sound and the radiation time (T_{II}) of the second heart sound, some discriminative steep pulses can be observed in these waveforms. Steep pulses at T_{II} were the mechanical vibrations caused by closure of the semilunar valves (the aortic and pulmonary valves) (Kanai 2007). The pulsive vibrations at T_I were mechanically caused vibrations due to closure of the atrioventricular valves (the mitral and tricuspid valves). These components at T_I and T_{II} correspond to the original vibrations of the two major heart sounds (the first heart sound and the second heart sound), which are audible using a stethoscope (Luisada and Portaluppi 1982). Especially during atrial systole, middle systole and the period of rapid inflow, there are small noisy components, which show the interaction between the rapid blood flow (inflow or outflow) and the heart wall.

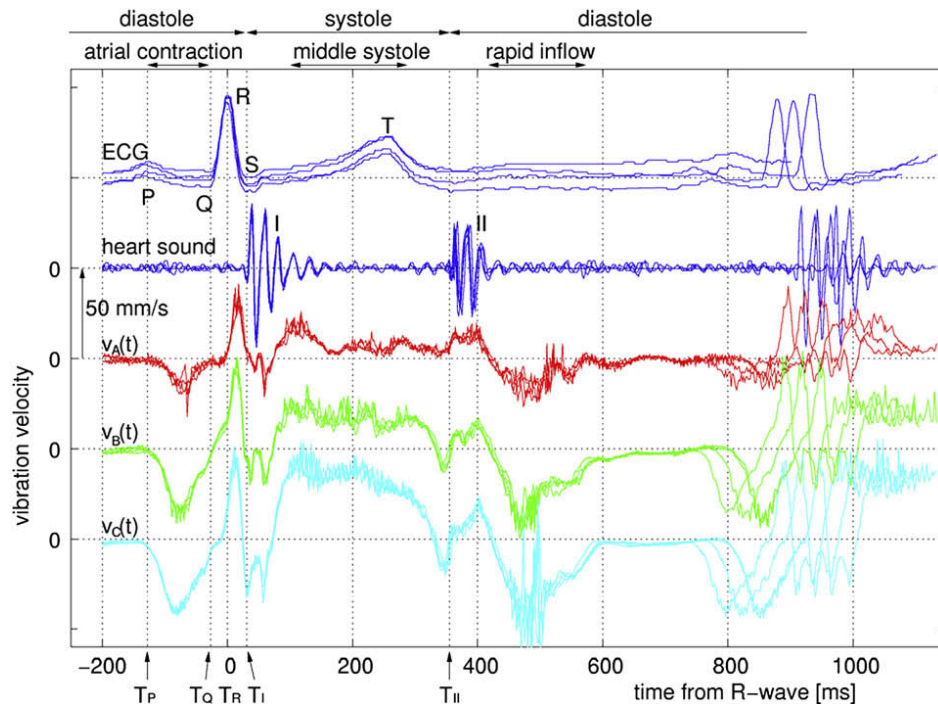


Fig 2. Vibration waveforms on the heart wall accurately measured at points A, B and C set in the interventricular septum (IVS) along an ultrasonic beam in Fig. 1a for a young healthy subject. The waveforms for four consecutive cardiac cycles are overlaid. Times T_Q , T_R , T_I and T_{II} , respectively, show the Q-wave and R-wave of the ECG, the beginning of the first heart sound and the beginning of the second heart sound.

Figures 2 through 4 show data for the above-mentioned subject. The ultrasonic beams were transmitted at every 2.25 degrees in eight directions ($N = 8$) and the pulse repetition interval $\Delta T = 1786 \mu s$, that is, the pulse repetition frequency (PRF) was 560 Hz and the temporal resolution in the measurement was about 2 ms. Figure 3 shows the consecutive instantaneous velocity distribution, $\{v_{j,k}(t)\}$ ($j = 1, 2, \dots; k = 4$), along the fourth ultrasonic beam which passes through the center of the IVS in Fig. 1a for a period of about ± 100 ms around the time (T_R) of the R-wave of the ECG. The horizontal red and blue bars show the upward velocity ($v_{j,k}(t) > 0$) and downward velocity ($v_{j,k}(t) < 0$), respectively.

For the same subject in Fig. 3, the consecutively obtained phase distributions are shown in the upper panel of each of Fig. 4a through c, in which the scales along the time and the depth axes exactly coincide with those in Fig. 3. In each of Fig. 4a through c, the upper panel shows the consecutive instantaneous phase distributions $\{\varphi_{j,k}(t; f_1)\}$ ($j = 1, 2, \dots; k = 4; |t - T_R| \leq 100$ ms) for the $f_1 = 21$ Hz, 41 Hz and 55 Hz components involved in the vibrations $\{v_{j,k}(t)\}$, simultaneously detected at several thousand points in the upright thin rectangular region of the heart wall of Fig. 1b. That is, the region surrounded by the upright thin black rectangle for each time was cut out and set in an array to show consecutive spatial distributions of color-coded phase values $\{\varphi_{j,k}(t; f_1)\}$ of the

waveforms along the center of the IVS around T_R , as shown in Fig. 4. The dashed straight lines, which correspond to the wave propagations in Fig. 3, are overlaid in Fig. 4. Since the low frequency component is dominant in the measured vibrations $\{v_{j,k}(t)\}$, the phase distribution $\{\varphi_{j,k}(t; f_1)\}$ in Fig. 4a corresponds to the velocity distribution $\{v_{j,k}(t)\}$ in Fig. 3. When a higher frequency of f_1 is employed in the Fourier transform, however, the wavelength of the sinusoidal wave component detected by the Fourier transform with f_1 becomes shorter and then the temporal resolution in the phase distributions $\{\varphi_{j,k}(t; f_1)\}$ increases; these phase distributions $\{\varphi_{j,k}(t; f_1)\}$ for higher frequency components ($f_1 = 41$ Hz and 55 Hz) are different from that ($f_1 = 21$ Hz) in Fig. 4a and the velocity distribution $\{v_{j,k}(t)\}$ in Fig. 3.

On the other hand, the region surrounded by the horizontal black rectangle in Fig. 1b was cut out, rotated by -90 degrees and set in an array to show the consecutive instantaneous phase distributions $\{\varphi_{j,k}(t; f_1)\}$ (j : fixed; k : varied; $|t - T_R| \leq 100$ ms) around T_R in the lower panel of each of Fig. 4a through c. Employing these panels, it is possible to show the propagation of the vibration in the transmural direction from the LV side to the RV side in the center of the IVS. For the propagation component which starts at the time of the Q-wave (T_Q) of the ECG, the propagation speed is 0.9 m/s, which corresponds to the conduction speed in the myocardium. On the other

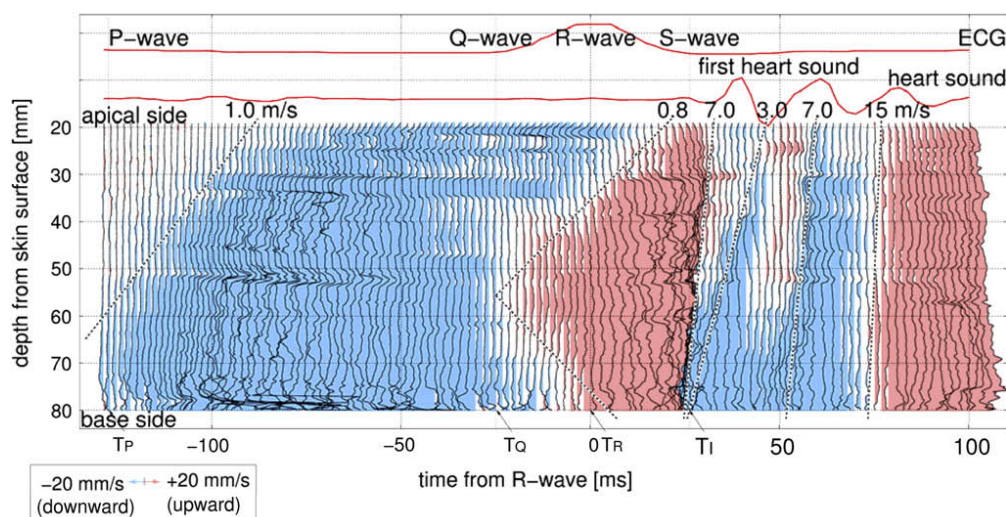


Fig. 3. Consecutive velocity distribution along an ultrasonic beam which passes through the center of the IVS in Fig. 1a for the period of about ± 100 ms around T_R of the same subject as in Fig. 2. The horizontal lengths of the red and blue bars show the upward velocity and downward velocity, respectively.

hand, for the components around T_I , there is no time delay between the LV and RV sides of the IVS.

The results obtained by applying the same procedures as those in Figs. 3 and 4 to two other healthy subjects are shown in Figs. 5, 6 and 7. Similar phenomena were observed for all three subjects. Since the duration of the first heart sound of the second subject (Figs. 5 and 6) was shorter than that of the first subject (Figs. 3 and 4), the number of wave propagations was less than that of the first subject. In Fig. 6b and c, at 130 ms and at 30 ms before T_Q , waves propagated twice from the base side of the IVS to the apical side with a propagation speed of 4 m/s, which corresponds to the conduction speed in the Purkinje fibers. A wave then propagated from each of a few points in the IVS to both apical and base sides of the IVS with a propagation speed of 0.9 m/s, which corresponds to the conduction speed in the myocardium. For the third subject in Fig. 7, however, these propagations started at about 200 ms and 100 ms before T_Q , the propagation phenomena of the wave which started at 100 ms before T_Q in Fig. 7 being similar to Figs 6b and c, and Fig. 4b and c.

DISCUSSION

The source of myocardial contraction is electrical stimulation. As shown in the vibration waveforms $v_A(t)$, $v_B(t)$ and $v_C(t)$ of Fig. 2, from the end of the first heart sound, these points move upward to the apical side and there are differences in amplitudes among these waveforms, which correspond to the speed of change in length. By integrating the difference between the waveforms, the changes in length between these points are obtained, which shows the contraction of the myocardium in the

IVS. However, contraction is obtained by integration along the time axis and, thus, the time resolution decreases. In Figs. 3 through 7, the displayed period is until the end of the first heart sound and, in this short period, no contraction is distinguishable.

As shown in Fig. 2, around T_Q , there were small inflection points in $v_A(t)$, $v_B(t)$ and $v_C(t)$. Around T_Q , mechanically caused vibration is not possible because the atrioventricular valves are still open. Physiologically, the depolarized action potentials, cyclically generated at the sino-atrial (SA) node, propagate through the atrioventricular (AV) node and His bundle to the Purkinje fibers. The Purkinje fibers form interweaving networks on the endocardial surface of both ventricles and transmit the cardiac impulse almost simultaneously to the right and left ventricular endocardia at a speed of 2–4 m/s (Zipes and Braunwald 2005; Katz 2001). Around T_Q , based on cell-to-cell connections, the action potential starts to propagate with a speed of 0.3–1 m/s (Katz 2001) to the entire heart wall from the Purkinje fiber-myocyte junctions on the surface of the IVS, where the Purkinje fibers are in contact with the myocardium. For the papillary muscle of a rat, the response of the myocardium to electrical stimulation can be detected as vibration velocity of the myocardium (Kanai et al. 2003). Thus, the vibration with inflection points around T_Q in Fig. 2 would correspond to the response of the myocardium in the IVS to the electrical stimulation.

As shown in Fig. 3, before T_Q , the downward (blue) components were dominant due to the ventricular dilatation during the atrial contraction. However, from T_Q , the region of the downward component was gradually replaced by the upward (red) component from the center

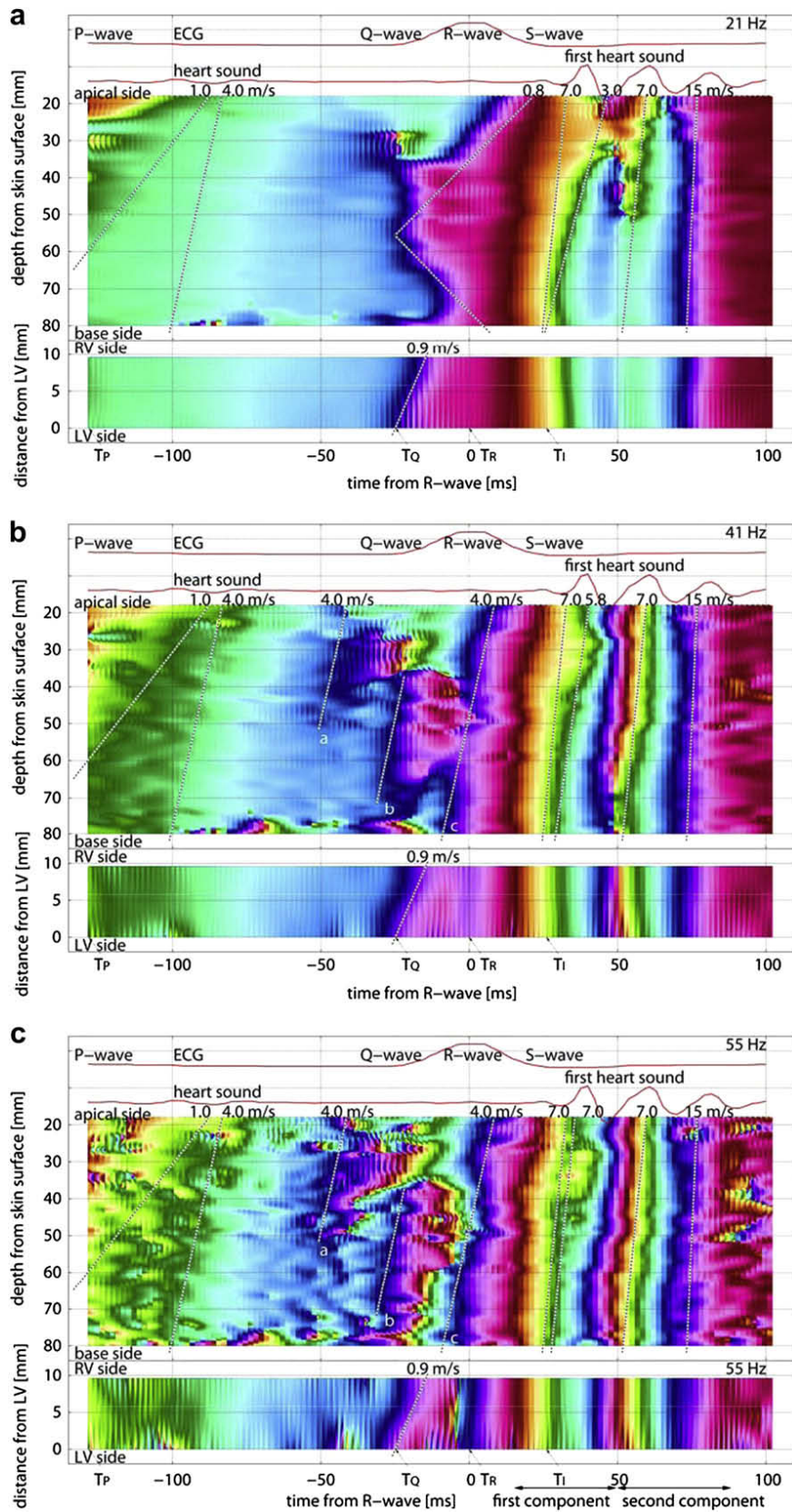


Fig. 4. Consecutive spatial distributions of color-coded phase values for the 22-Hz (a), 42-Hz (b) and 55-Hz (c) components of the measured waveforms for the subject in Figs. 2 and 3. The upper panel of each figure shows the consecutive distribution along the center of the IVS from the apex to the base. The lower panel of each figure shows the consecutive distribution in the transmural direction from the LV side to the RV side. At least the same dotted straight lines corresponding to the propagation in Fig. 3 are overlaid in Fig. 4a.

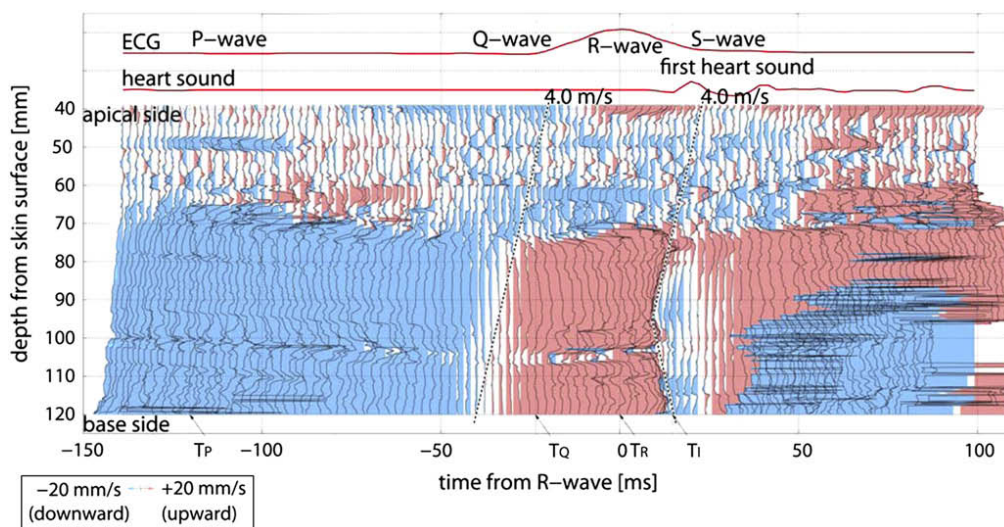


Fig. 5. Consecutive velocity distribution of the second healthy young subject for the period of about ± 100 ms around T_R along an ultrasonic beam, which passes through the center of the IVS as in Fig. 1a. The horizontal lengths of red and blue bars show the upward velocity and downward velocity, respectively.

part of the IVS to both the base and apical sides. Since its propagation speed was slow at about 0.8 m/s, which corresponds to the conduction speed in the myocardium, this phenomenon would correspond to the muscle contraction caused by the depolarization of the heart muscle. At the radiation time (T_I) of the first heart sound, the velocity distribution became complex due to propagation of several vibrations corresponding to the heart sound. Then, 70 ms after T_R , the upward (red) component became dominant, reflecting the contraction of the ventricle in systole. The propagation speeds of the vibrations corresponding to the first heart sound were 3–15 m/s. Since the vibration was measured in the axial direction of the ultrasound and its direction was the same as the wave propagation along the IVS, the measurement was inconsistent with the definition of a shear wave. By separate *in vivo* experiments, from the parasternal longitudinal axis view of the IVS, there were some wave propagations from the time of the R-wave and the propagation speed of each component was on the order of several m/s. Though the IVS is narrow, there is possibility that the wavefront inclined by several degrees from the axis passing through the IVS and from the axial direction of the measured ultrasound. Due to these factors, these vibrations correspond to the shear wave (Kanai 2005; Kundo 2003; Sarvazyan et al 1995). It was found for the first time in the present study that two or three pulses propagate with different speeds along the IVS.

In the upper panel of Fig. 4a, phenomena similar to those of Fig. 3 were observed because the low frequency components were dominant in the detected vibrations. Before T_Q , blue or green components, which show the downward components according to the upper-right

circular illustration in Fig. 1b, were dominant. From T_Q in the upper panel of Fig. 4a, a wave (violet: 270-degree component of a sinusoidal wave) began to propagate from the center of the IVS to both sides. The dotted straight lines in Fig. 4a coincide with those in Fig. 3. Another propagation is shown in Fig. 4a, which started 100 ms before the R-wave and propagated at a speed of 4 m/s. In Fig. 4b and c, a similar propagation was found. For this subject, the peak time T_P of the P-wave of the ECG was 130 ms before the R-wave. Thus, after the time of the P-wave, a pulse propagated from the base side to the apical side at a speed of 4 m/s, corresponding to that of the conduction speed in the Purkinje fibers.

By increasing the temporal resolution using higher frequency analysis in the upper panel of Fig. 4b and c, at 50 ms after the propagation, there were three waves, which started at points a, b and c in the upper panel of Fig. 4b and c. Their propagation speed was about 4 m/s. These phenomena are very complex and are considered to show the response of the myocardium to the excitation due to the propagation of the electrical conduction wave. Though there are a few propagations, which correspond to the propagation of the electrical conduction wave from the viewpoint of propagation speed, direction and time, these differences and causes could not be clarified in the present study.

Then, from 12 ms after T_R , the upward (red) component clearly propagated from the base of the IVS to the apical side. Its speed was about 7 m/s and did not vary for the frequencies of 21 Hz, 41 Hz and 55 Hz. This would be the shear wave mechanically caused by closure of the atrioventricular valves. The reason why the propagation speed was unchanged at different frequencies for a shear

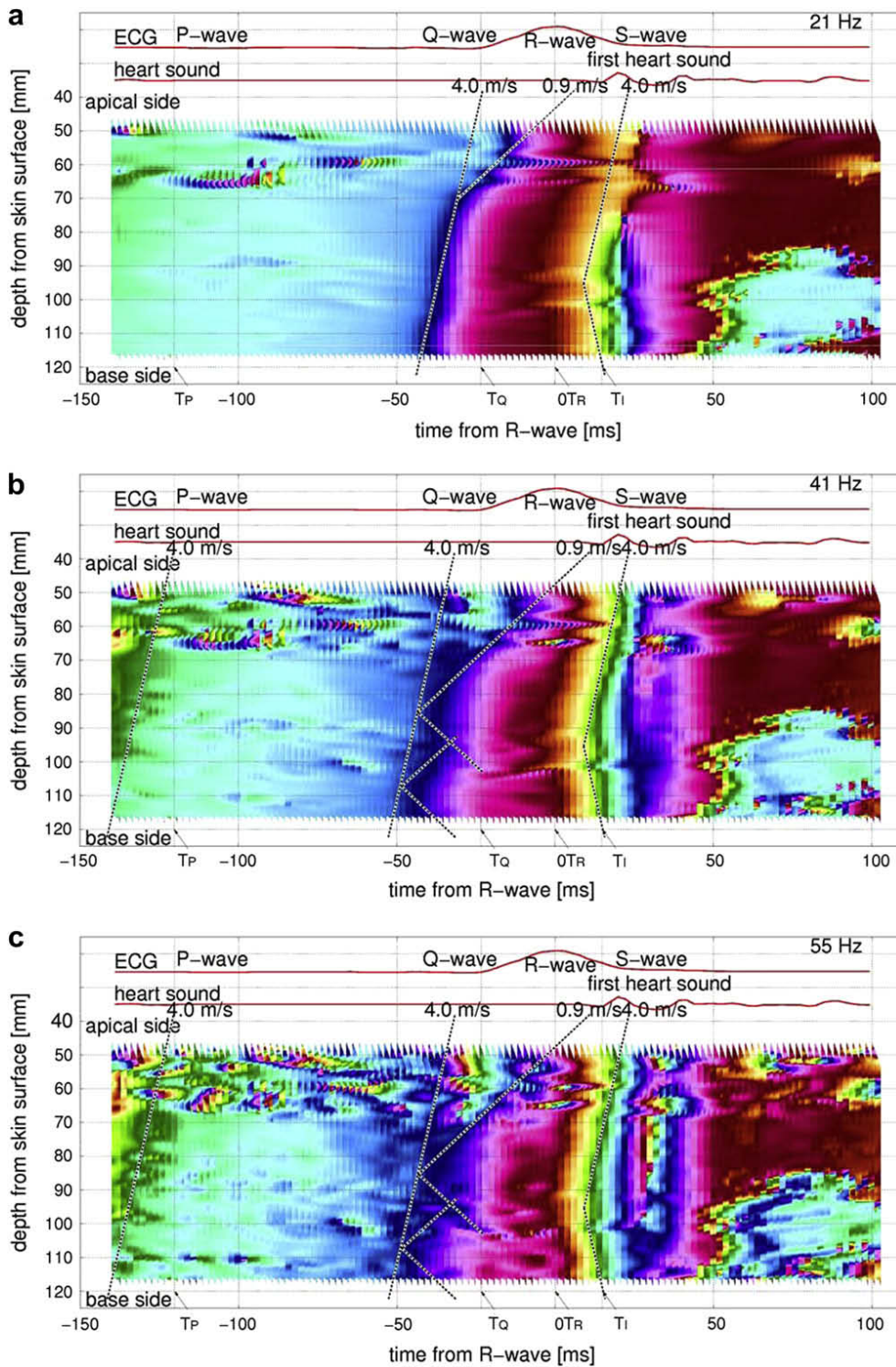


Fig. 6. Consecutive spatial distributions of the color-coded phase values of the waveforms along the center of the IVS around T_R for the 22-Hz (a), 42-Hz (b) and 55-Hz (c) components for the second subject in Fig. 5.

wave is described in the next paragraph. At T_I (about 30 ms after T_R), the two components (yellow and green components) started to propagate in the same direction. The yellow component is clearly shown in Fig. 4 and

the propagation speed is 7.0 m/s. For the green component, however, there was large dispersion since its speed was about 3.0 m/s for 21 Hz, 5.8 m/s for 41 Hz and 7.0 m/s for 55 Hz. Thus, this would be the Lamb wave, a shear

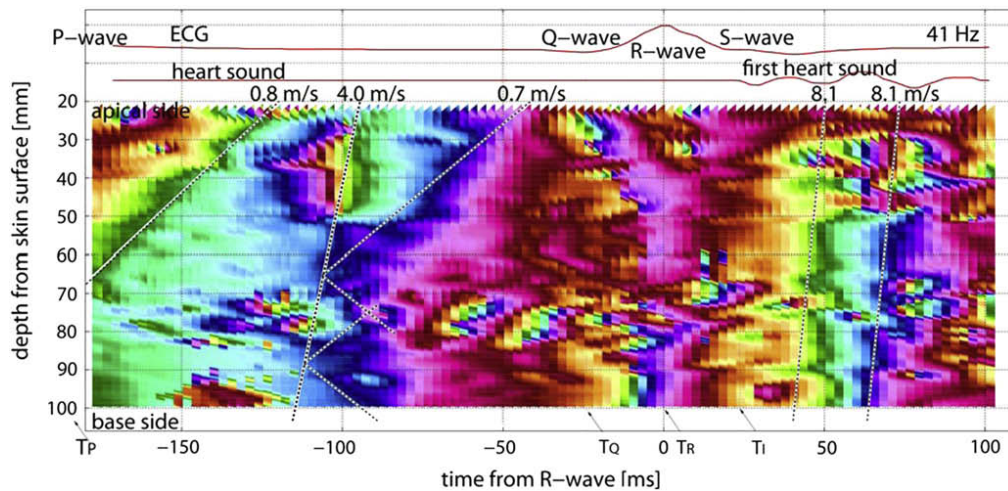


Fig. 7. Consecutive spatial distributions of the color-coded phase values of the waveforms along the center of the IVS around T_R for the 42-Hz component for the third healthy young subject.

horizontal wave of the guided wave in a thin wall (the septum), which was mechanically caused by closure of the atrioventricular valves. The propagation of this mechanically caused vibration was also observed at the radiation time of the second heart sound in a previous study (Kanai 2005), in which the pulse propagated from the root of the aortic valve to both the base side and the apical side at the time of the aortic valve closure. The dispersion property for the Lamb wave is determined by the geometric dispersion and the viscous dispersion. As shown in the upper panel of Fig. 4b and c, from 50 ms after T_R , the second component of the first heart sound propagated in the same direction. The propagation speed was about 7 m/s and there was no clear dispersion. In Fig. 4a, the propagation of the second component cannot be clearly detected since the temporal resolution is not so high for the low frequency component.

For the shear wave, its propagation speed at the angular frequency ω depends on the complex viscoelastic modulus $G^*(\omega)$, which is composed of the storage modulus $G_R(\omega)$ and the loss modulus $G_I(\omega)$, the latter being given by the viscosity $\mu_2(\omega)$ multiplied by ω . There have been few data on the human myocardium, which could be used to determine the frequency dependence of such mechanical properties. Alternatively, according to the measured data for the thoracic arterial walls of human subjects (Learoyd et al. 1966), for the frequency range of 2 to 10 Hz, the storage modulus $G_R(\omega)$ and loss modulus $G_I(\omega)$ are almost unchanged, which means that the viscosity $\mu_2(\omega) = G_I(\omega)/\omega$ gradually decreased as the frequency increased. However, the rate of decrease was not given in the cited paper. Nasseri et al. 2002 quantitatively determined the frequency dependency of the viscosity $\mu_2(\omega)$ of pig kidney to be $2362.6 \times \omega^{(0.278-1)} = 626.7 \times f^{-0.722}$ [Pa·s], where this relationship well

describes the frequency dependence of the above viscosity $\mu_2(\omega)$ for the human thoracic artery (Learoyd et al. 1966). Thus, it can be assumed that the loss modulus $G_I(\omega) = \omega \times \mu_2(\omega)$ of the human heart is in proportion to $\omega \times \omega^{-0.722} = \omega^{0.278}$. When the stiffness ratio $G_I(\omega)/G_R(\omega)$ is assumed to be about 0.8, which was measured for the canine left ventricle in case of 120 mmHg by pressure perturbation at 22 Hz (Templeton and Nardizzi 1974), the change in the magnitude of the elastic modulus $|G^*(\omega)| = |G_R(\omega) + jG_I(\omega)|$ can be roughly estimated to be $|G^*(55 \text{ Hz})|/|G^*(21 \text{ Hz})| \cong 1.13$. That is, in the frequency range of 21 Hz to 55 Hz measured in the present study, $|G^*(\omega)|$ is almost unchanged and thus the propagation speed of the shear wave appears to be unchanged. For the present procedure, it is difficult to accurately measure the propagation speed to differentiate these small changes. For the Lamb wave, on the other hand, its propagation speed depends on the viscous dispersion determined by elastic modulus $G^*(\omega)$ and geometric dispersion.

The wave propagations in the lower panel in each of Fig. 4a through c correspond to those found in the upper panel of each of the figures. However, there was a time delay for the component at T_Q , which means that the component propagates from the LV side to the RV side at a speed of about 1 m/s, which corresponds to the conduction speed in the myocardium. For the two vibration components corresponding to the first heart sound, there was no clear time delay. Thus, the wavefront of each of the latter components is perpendicular to the axis of the apex-base along the IVS. In the upper panel of each of Fig. 4a through c, the green component which starts at a time T_I has a large dispersion property, which would be the Lamb wave. On the other hand, in the lower panels of Fig. 4a through c, there are corresponding green components. However, as the thickness of the IVS is

about 10 mm, it is difficult to detect the incline angle of the wave front from the axis passing through the septum and from the axial direction of the measured ultrasound.

The bundles of His have two branches, on the left ventricular side and right ventricular side, respectively, and on both sides there are Purkinje fibers. Thus, from the physiologic point of view, it is normally considered that the electrical conduction wave propagates from both sides to the middle of the IVS. However, the *in vivo* experimental results obtained in the present study do not correspond to these physiologic facts. This should be clarified in future studies.

At 20 ms before T_Q in Fig. 6 and at 90 ms before T_Q in Fig. 7, a wave propagated from the base side of the IVS to the apical side with a propagation speed of about 4 m/s, which corresponds to the conduction speed in the Purkinje fibers. Then, from each of the several points in the IVS, a wave propagated to both the apical and base sides of the IVS with a propagation speed of about 0.9 m/s, which corresponds to the conduction speed in the myocardium. These results show the possibility that the detected phenomena correspond to the response of the myocardium to the excitation due to the propagation of an electrical conduction wave. Since it is known that simple bifurcation of the Purkinje fibers into the anterior and posterior fascicles is uncommon (Katz 2001) and highly depends on the subjects, such differences among the three subjects regarding the propagation around T_Q will occur. According to the rough sketch by Netter 1969, the electrical conduction wave arrives at the IVS at about the same time as the Q-wave of the ECG. Thus, for the subjects in Figs. 4 and 6, the above results correspond to the physiologic phenomenon. However, for the subject in Fig. 7, the arrival time of the electrical conduction wave was much earlier than that of the Q-wave, which is also one of the problems unresolved in the present study.

Since the propagation time of these components is very short, *i.e.*, about 10 ms from the base to the apex, it has been difficult to measure and analyze these phenomena. For noninvasive electrocardiographic imaging for cardiac electrophysiology and arrhythmia (Ramanathan et al 2004), the estimation of the potential is restricted to the surface of the heart wall (epicardium) and, thus, the potential inside the IVS cannot be estimated. Even with the excellent MRI-tagging method (Wyman et al. 1999a, 1999b; Zwanenburg et al. 2004), the spatial and time resolutions are still not sufficient. These phenomena are very complex and it is still difficult to completely explain the relationship between these vibrations and either the ECG or the heart sound, which was detected as a longitudinal wave by a microphone attached to the chest wall.

In Figs. 3 through 7, the analyzed period, *i.e.*, from the P-wave of the ECG to the S-wave of the ECG, is about 200 ms around the time (T_R) of the R-wave. During this

short period in end diastole, the wall moves slowly and the displacement is very small. The displacement component along the ultrasonic beam can be tracked by measurement. The displacement component normal to the ultrasound beam in the apical view can be estimated from the displacement along the ultrasonic beam in the parasternal longitudinal view as shown in Fig. 1b of Kanai 2005. For example, for the period just before the R-wave of the ECG, there is a small downward pulse in the parasternal longitudinal view. For this pulse, the maximum amplitude is about 50 mm/s at the middle septum but the duration time is about 50 ms. By approximating the velocity waveform of this pulse with a downward isosceles triangle, the displacement accumulated during the period can be estimated to be about $(50 \text{ mm/s}) \times (50 \text{ ms})/2 \cong 1.3 \text{ mm}$, which is comparable to the size (about 1.5 mm) of the focal area. Thus, it can be assumed that the each myocardium does not move so much as the focal area of the ultrasonic beam during this short period. In Figs. 3 through 7, moreover, since the analyzed period for each propagation is at most 50 ms, it can be assumed that the each propagation phenomenon is shown for the same myocardium. These assumptions should be further clarified by simultaneous measurements of various components in the displacement.

The accuracy has been evaluated for the velocity measurement (Kanai et al. 1997) and for minute change in thickness (Kanai et al. 1999b). When the signal-to-noise ratio (SNR) is low such as in obese subjects, a decrease in the accuracy is inevitable. However, the relationship among the SNR in an acquired RF signal, the accuracy in the velocity measurement and the accuracy in the phase estimate of the velocity waveform have not been evaluated. The decrease in the SNR for the suboptimal images in actual clinical measurements has not been evaluated either. These evaluations should be established in the near future for actual clinical application.

The velocity of each wave propagation shown in Figs. 3 through 7 was determined by dividing the distance (vertical axis) by the propagation time. The dashed line was drawn manually by considering the wave front visible in Fig. 2. The emphasis of this study is not on the accurate determination of the wave velocity but on the fact that there are several wave propagations in the septum at around the R-wave of the ECG. Thus, the velocity values were expressed as two digits in this study. It is necessary for clinical applications to develop a method to determine the propagation velocity of each wave in the results as in Figs. 3 through 7.

Infarcted muscle, resulting from an occluded coronary artery, is already dead and so polarization of the cells is not possible. Between the infarcted area and the surrounding normal muscle, there is injured cardiac muscle, which has cell membranes that are never fully

polarized due to the deficiency of ion channel gating (Netter 1969). In such injured myocardium, the conduction speed decreases. Moreover, during the remodeling from the onset of acute myocardial infarction to the chronic stage, myocardial mechanical properties (acoustic velocity and attenuation) change (Saijo *et al.* 1997). Since each of these propagations depends on the regional myocardial characteristics, that is, the physiologic properties of the action potential and the mechanical properties of the viscoelasticity, both of which cannot be noninvasively estimated in general, new insights on these spontaneous phenomena detected in human subjects in this study show potential for noninvasive assessment of myocardial tissue damage due to heart failure and its spatial range. The method also has potential as a noninvasive tool for assessing de-synchronization of myocardial function in cardiac fibrillation as in Witkowski *et al.* 1998 and Rohr *et al.* 1997.

CONCLUSION

To conclude, by observing rapid, minute vibration components simultaneously at several thousand points in the human heart wall to visualize the wave propagation along the heart wall, we found for the first time that there are several types of vibration propagation which start at T_Q and T_I . By considering the time, the propagation direction and the dispersion properties of each vibration, the vibration at T_Q was seen to correspond to the response of the myocardium to electrical stimulation, which propagates from the Purkinje fiber-myocyte junctions to the whole heart and the vibrations at T_I correspond to the propagation of the waves mechanically excited by closure of the atrioventricular valves. These phenomena have potential for detection of regional myocardial tissue damage related to propagation of the action potentials and regional myocardial viscoelasticity.

Acknowledgments—The author is grateful to Prof. Yoshifumi Saijo of Tohoku University for his helpful and valuable advice. The author is also grateful to Prof. Emeritus Motono Tanaka of Tohoku University, Prof. Floyd Dunn of the Bioacoustics Research Laboratory of the University of Illinois and Dr. Jens E. Wilhjelm of the Technical University of Denmark for useful discussions. The author also acknowledges the experimental contributions of Assoc. Prof. Dr. Hideyuki Hasegawa in our laboratory.—This study was partly supported by a grant-in-aid for scientific research from the Ministry of Education, Culture, Sports, Science and Technology of Japan (2005–2007, No. 17206043).

REFERENCES

- Axel L, Dougherty L. MR imaging of motion with spatial modulation of magnetization. *Radiology* 1989;171:841–845.
- Buchalter MB, Weiss JL, Rogers WJ, Zerhouni EA, Weisfeldt ML, Beyar R, Shapiro EP. Noninvasive quantification of left ventricular rotational deformation in normal humans using magnetic resonance imaging myocardial tagging. *Circulation* 1990;81:1236–1244.
- Durrer D, van Dam RT, Freud GE, Janse MJ, Meijler FL, Arzbaecher RC. Total excitation of the isolated human heart. *Circulation* 1970;41:899–912.
- Fleming AD, Xia X, McDicken WN, Sutherland GR, Fenn L. Assessment of colour Doppler tissue imaging using test-phantoms. *Ultrasound Med Biol* 1994;20:937–951.
- Heimdal A, Støylen A, Torp H, Skjærpe T. Real-time strain rate imaging of the left ventricle by ultrasound. *J Am Soc Echocardiogr* 1998;11:1013–1019.
- Kanai H, Sato M, Koiwa Y, Chubachi N. Transcutaneous measurement and spectrum analysis of heart wall vibrations. *IEEE Trans Ultrason Ferroelectr Freq Control* 1996;43:791–810.
- Kanai H, Hasegawa H, Chubachi N, Koiwa Y, Tanaka M. Noninvasive evaluation of local myocardial thickening and its color-coded imaging. *IEEE Trans Ultrason Ferroelectr Freq Control* 1997;44:752–768.
- Kanai H, Koiwa Y, Zhang J. Real-time measurements of local myocardium motion and arterial wall thickening. *IEEE Trans Ultrason Ferroelectr Freq Control* 1999a;46:1229–1242.
- Kanai H, Sugimura K, Koiwa Y, Tsukahara Y. Accuracy evaluation in ultrasonic-based measurement of microscopic change in thickness. *Electron Lett* 1999b;35:949–950.
- Kanai H, Yonechi S, Susukida I, Koiwa Y, Kamada H, Tanaka M. Onset of pulsatile waves in the heart walls at end-systole. *Ultrasonics* 2000;38:405–411.
- Kanai H, Koiwa Y. Myocardial rapid velocity distribution. *Ultrasound Med Biol* 2001;27:481–498.
- Kanai H, Katsumata S, Honda H, Koiwa Y. Measurement and analysis of vibration in the myocardium telescopic motion for novel echographic diagnosis. *Acoust Sci Technol* 2003;24:17–22.
- Kanai H. Propagation of spontaneously actuated pulsive vibration in human heart wall and *in vivo* viscoelasticity estimation. *IEEE Trans Ultrason Ferroelectr Freq Control* 2005;52:1931–1942.
- Kanai H. Ultrasonic imaging of propagation of electric excitation in heart wall. *IEEE Ultrason Symp* 2007;753–756.
- Katz AM. *Physiology of the Heart*. Philadelphia: Lippincott Williams & Wilkins; 2001.
- Konofagou E, Luo J, Saluja D, Fujikura K, Cervantes D, Coromilas J. Noninvasive electromechanical wave imaging and conduction velocity estimation *in vivo*. *IEEE Ultrason Symp* 2007;969–972.
- Kundo T. *Ultrasonic nondestructive evaluation*. New York: CRC Press; 2003.
- Learoyd BM, Taylor MG. Alterations with age in the viscoelastic properties of human arterial walls. *Circ Res* 1966;18:278–292.
- Luisada AA, Portaluppi F. *The heart sounds: New facts and their clinical Implications*. New York: Praeger Scientific; 1982.
- Mahoney LT, Smith W, Noel MP, Florentine M, Skorton DJ, Collins SM. Measurement of right ventricular volume using cine computed tomography. *Invest Radiol* 1987;22:451–455.
- Nasseri S, Bilston LE, Phan-Thien N. Viscoelastic properties of pig kidney in shear, experimental results and modelling. *Rheologica Acta* 2002;41:180–192.
- Netter FH. *A compilation of paintings on the normal and pathologic anatomy and physiology, embryology, and diseases of the heart*. Summit, NJ: Ciba Pharmaceutical; 1969.
- Notomi Y, Setser RM, Shiota T, Martin-Miklovic MG, Weaver JA, Popovic ZB, Yamada H, Greenberg NL, White RD, Thomas JD. Assessment of left ventricular torsional deformation by Doppler tissue imaging: Validation study with tagged magnetic resonance imaging. *Circulation* 2005;111:1141–1147.
- Pernot M, Fujikura K, Fung-Kee-Fung SD, Konofagou E. ECG-gated, mechanical and electromechanical wave imaging of cardiovascular tissues *in vivo*. *Ultrasound Med Biol* 2007;33:1075–1085.
- Ramanathan C, Ghanem RN, Jia P, Ryu K, Zudy Y. Noninvasive electrocardiographic imaging for cardiac electrophysiology and arrhythmia. *Nat Med* 2004;10:422–428.
- Rohr S, Kucera JP, Fast VG, Kléber AG. Paradoxical improvement of impulse conduction in cardiac tissue by partial cellular uncoupling. *Science* 1997;275:841–844.
- Saijo Y, Tanaka M, Okawai H, Sasaki H, Nitta S, Dunn F. Ultrasonic tissue characterization of infarcted myocardium by scanning acoustic microscopy. *Ultrasound Med Biol* 1997;23:77–85.

- Sarvazyan AP, Skovoroda AR, Emelianov SY, Fowlkes JB, Pipe JG, Adler RS, Buxton RB, Carson PL. Biophysical bases of elasticity imaging. *Acoust Imaging* 1995;21:223–240.
- Sutherland GR, Stewart MJ, Groundstroem KW, Moran CM, Fleming A, Guell-Peris FJ, Riemersma RA, Fenn LN, Fox KA, McDicken WN. Color Doppler myocardial imaging: A new technique for the assessment of myocardial function. *J Am Soc Echocardiogr* 1994;7:441–458.
- Templeton GH, Nardizzi LR. Elastic and viscous stiffness of the canine left ventricle. *J Appl Physiol* 1974;36:123–127.
- Wang S, Lee WN, Provost J, Luo J, Konofagou EE. A composite high-frame-rate system for clinical cardiovascular imaging. *IEEE Trans Ultrason Ferroelectr Freq Control* 2008;55:2221–2233.
- Witkowski FX, Leon LJ, Penkoske PA, Giles WR, Spanok MR, Ditto WL, Winfree AT. Spatiotemporal evolution of ventricular fibrillation. *Nature* 1998;39:78–82.
- Wyman BT, Hunter WC, Prinzen FW, McVeigh ER. Mapping propagation of mechanical activation in the paced heart with MRI tagging. *Am J Physiol Heart Circ Physiol* 1999a;276:881–891.
- Wyman BT, Hunter WC, Prinzen FW, Faris OP, McVeigh ER. Effects of single- and biventricular pacing on temporal and spatial dynamics of ventricular contraction. *Am J Physiol Heart Circ Physiol* 1999b;282:H372–H379.
- Yoshiara H, Hasegawa H, Kanai H, Tanaka M. Ultrasonic imaging of propagation of contraction and relaxation in the heart walls at high temporal resolution. *Jpn J Appl Phys* 2007;46:4889–4896.
- Zipes DP, Braunwald E. *Braunwald's Heart disease: A textbook of cardiovascular medicine*. Philadelphia: Elsevier; 2005.
- Zwanenburg JJM, Götte MJM, Kuijper JPA, Hofman MBM, Knaapen P, Heethaar RW, van Rossum AC, Marcus JT. Reduction in postsystolic wall thickening during late preconditioning. *Am J Physiol Heart Circ Physiol* 2004;288:787–794.